EUROFUSION WP14ER-PR(16) 15923

A. Curcio et al.

Imaging plates calibration to X-rays

Preprint of Paper to be submitted for publication in
Journal of Instrumentation

This work has been carried out within the framework of the EUROfusion Consortium and has received funding from the Euratom research and training programme 2014-2018 under grant agreement No 633053. The views and opinions expressed herein do not necessarily reflect those of the European Commission.

Imaging plates calibration to X-rays

A. Curcio,[a,*] P. Andreoli[b], M. Cipriani[b], G. Claps[b], F. Consoli[b] , G. Cristofari[b], R. De Angelis[b], D. Giulietti[c], F. Ingenito[b] and D. Pacella[b]

[a]*Physics Department of the Roma University "La Sapienza", P.le A. Moro n.5, Roma, Italy ,*
[b]*ENEA for EUROfusion, via E. Fermi 45, 00044 Frascati (Rome), Italy*
[c]*Physics Department of the University and INFN, Largo Bruno Pontecorvo, 3 56127 Pisa, Italy*

E-mail: Alessandro.Curcio@uniroma1.it

ABSTRACT: The growing interest for the Imaging Plates, due to their high sensitivity range and versatility, has induced, in the last years, to detailed characterizations of their responce function in different energy ranges and kind of radiation/particles. A calibration of the Imaging Plates BAS-MS, BAS-SR, BAS-TR has been performed at the ENEA-Frascati labs by exploiting the X-ray fluorescence of different targets (Ca, Cu, Pb, Mo, I, Ta) and the radioactivity of a BaCs source, in order to cover the X-ray range between few keV to 80 keV.

KEYWORDS: Imaging Plates; IP response function; X-rays.

Corresponding author.

Contents

1. Introduction

Imaging plates are two-dimensional X-ray/particle detectors which have acquired more and more importance during the last years in the fields of medicine, physics, and biology. Their chemical composition is the rare-earth-doped alkaline-earth halide $BaFBr:Eu^{2+}$ often with a small addition of iodine. The storing mechanism by which a latent image is obtained after X-ray exposure of the plate is the trapping of information in locally electron-hole bound state. Information is recovered by photostimulated luminescence, namely by radiating the IP with a red laser (HeNe typically), then collecting a 3.2 eV photon that results from the Eu^{2+} transition $4f^6\ 5d \rightarrow 4f^7$ [1,2]. Imaging plates can offer precious performances in X-rays and particles detection insofar they have a really high dynamical range (up to six order of magnitude), spatial resolution, a linear response to the radiation dose and the wonderful advantage to be reusable many times. Calibrations in literature can be found to particles [3,4,5,6,7,8] and to X-rays [9,10,11]. They consist in the exposure of the plates to different photon or particle energies and in the measurement of the level of exposure given in Photo Stimulated Luminescence (PSL). The PSL is the number of photons emitted in the reading process of the exposed plates to a certain energy of particles or photons. Of course this number can depend strongly not only to the proper response of the plate material but also to the time passing between the exposure and the reading. In fact a fading time characteristic curve is associated to the different kind of imaging plates in commerce [8]. Also the scanner used to read the imaging plates can play an important role in determining the PSL value due to the performances of the HeNe installed inside, which can vary from scanner to scanner. The importance of calibration curves giving the response function of these detectors lays in the fact that so versatile plates, passive detectors undisturbed by electromagnetic noise, are in effect very suitable for laser plasma experiments, both in experiment of inertial confinement and in ion/electrons acceleration, namely for high energy long pulses (nanoseconds) down to femtosecond high intensity laser pulses. The utilization of the imaging plates can be multiple, from imaging to spectrometry. In the case of

photon detection the imaging plates are useful for imaging when are coupled to a pin-hole camera for example, while in the case of spectrometry they can be coupled with a Bragg crystal or a grating in order to induce dispersion and measure directly X-ray spectra. In the case of particle detection they can be used to measure directly particle bunch distributions as well as coupled with a dipole or a Thomson parabola they can be used to directly measure particle energy spectra. The possibility to use different metallic or plastic filters with different thickness both in detecting particle or radiation is allowed in order to get a simultaneous measurement of spatial distribution and spectrum (after a deconvolution method [12]). About calibrations to date not all the ranges of particles and radiation have been explored, especially for photons the range of low energies around 1 keV, very appealing for laser-fusion experiments, and for ions, very often present in experiments of ion acceleration via laser.

2. Three types of Imaging Plates

After having shortly explained the working principles of the IP, we make an overview of the various types of imaging plates actually in commerce, supplied by GE Healthcare corporation. We'll show some tables with specifications. The protective layers are generally made out of Mylar films (technically Polyethylene terephthalate), a thermoplastic polymer resin of the polyester family. About the phosphor layer, which constitutes the sensible part of the IP as detector, several things have been already said. The support layer is usually made of Mylar too, and its function is just to give more rigidity to the detector, while the ferrite layer ($ZnMn_2$ Fe_5 NO_{40} H_{15} C_{10}) is thought for medical application in which magnetic attachments are needed.

2.1 BAS-MS type

They are the most sensitive and have an high resistance to water [11]. The phosphor layer composition is ($BaFBr_{0.85}$ $I_{0.15}$:Eu^{2+}). The characteristics are shown in Table 1:

Table 1: BAS-MS characteristics [1].

Protective layer	9 μm
Phosphor layer	115μm
Support layer	190 μm
Magnetic layer	160 μm

2.2 BAS-SR type

They have the greatest resolution and have an high resistance to water [11]. Its phosphor layer composition is (BaFBr:Eu^{2+}). The characteristics are shown in table 2:

Table 2: BAS-SR characteristics [1].

Protective layer	6 μm
Phosphor layer	120μm
Support layer	188 μm
Magnetic layer	160 μm

2.3 BAS-TR type

They are the most appropriate for ^{3}H detection, don't have a protective layer, thus they are the most sensitive to malfunctions due to humidity [11]. Its phosphor layer composition is ($BaFBr_{0.85}\ I_{0.15}:Eu^{2+}$). The characteristics are shown in table 3:

Table 3: BAS-TR characteristics [1].

Protective layer	0 μm
Phosphor layer	50μm
Support layer	250 μm
Magnetic layer	160 μm

3. Absolute calibration of Imaging Plates to X-rays

Imaging plates as X-rays detectors can realize their optimal performances when absolutely calibrated. An absolute calibration would provide the real number of photons per unit surface and with further tricks their energy, i.e. information about the radiation spectra, that together with the high spatial resolution (which IP naturally offer) make them very interesting detection devices.

3.1 Sources and detectors

The absolute calibration of IP is only possible with an absolutely calibrated X-rays source, with which one can irradiate the imaging plates with a completely known radiation signal. A new X-ray laboratory [13] has been built in Frascati (ENEA) to develop diagnostics for nuclear fusion experiments and other studies or applications. This lab provides two absolutely calibrated source of X-rays: first the soft X-rays source (model Moxtek 50 kV Bullet, fig. 1) with Ag anode, variable high voltage in the range 10÷50 kV, and current in the 1÷200 μA range, 1 μA precision and stability better than 1%; the second source is the high-voltage Micro focus (model Oxford Instruments SB-80-1M, fig. 2), characterized by having a tungsten anode, variable voltage in the range 35÷80 kV and current in the 10÷1000 μA, focal spot size of 33 μm. In fig. 1, the spectrum of the Moxtek source at 15 kV, acquired with Si-PIN diode located at 100 mm from the source and limited by a pinhole, is shown (blue line). The calculated spectral distribution at the exit of the source (fig. 1, green line) is obtained with a home-made code allowing the calculation of the spectrum with any choice of filter, distance, slit by including air absorption, solid angle, pinhole, detection efficiency of the Si-PIN and acquisition time. The correction of the air absorption causes a divergence at low energy and for this reason a cutoff at 4 keV is defined. The spectrum at the exit of the source is extrapolated linearly up to 0 keV and the effect of the Be window (250 μm thick) is then applied (fig. 1, red curve). Since the measured spectrum is 4 orders of magnitude less than the reconstructed spectra at the exit, it is multiplied by 2098, an arbitrary number, to be plotted in the same scale of the others. The fitted spectrum is different from the measured spectrum because it represents the spectrum at the exit of the source, while the measured spectrum is affected by the air absorption and pin-hole cuts.

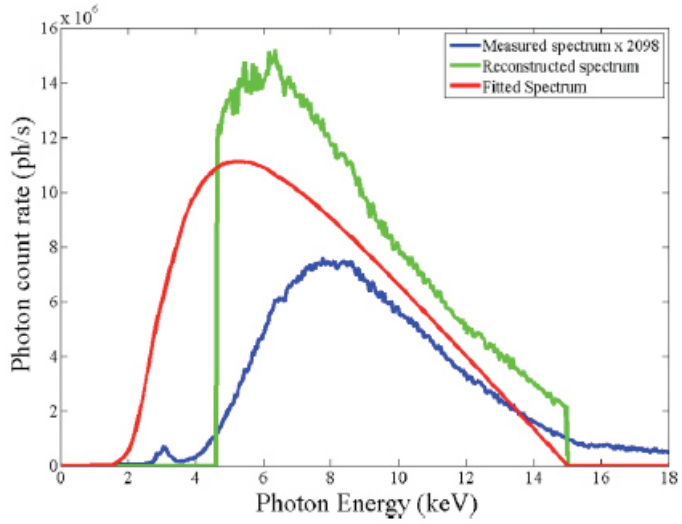

Figure 1: Spectrum of Moxtex X-ray source [13] with voltage set at 15 kV and current at 50 µA. The blue line is the spectrum measured at 100 mm and limited by a pinhole. The reconstructed spectral distribution at the exit of the source is the green line, where the cutoff at 4 keV is due to the air absorption of low energies that generates singularities in calculations. The fitted red spectrum takes into account the air absorption of energies below 4 keV and of the Be window at the source exit.

In fig. 2 measured spectra (blue curves) and reconstructed ones (red curves) at 35 and 80 kV are shown, relative to the Micro focus source. The reconstructed spectrum and the fitted spectrum are very similar like in the case of the Moxtex source; in this case, at higher photon energies, we don't have to take into account the air absorption induced cutoff. The measured spectrum is multiplied by 10^5, an arbitrary number, in order to have it in the same scale of the other curves in the frame.

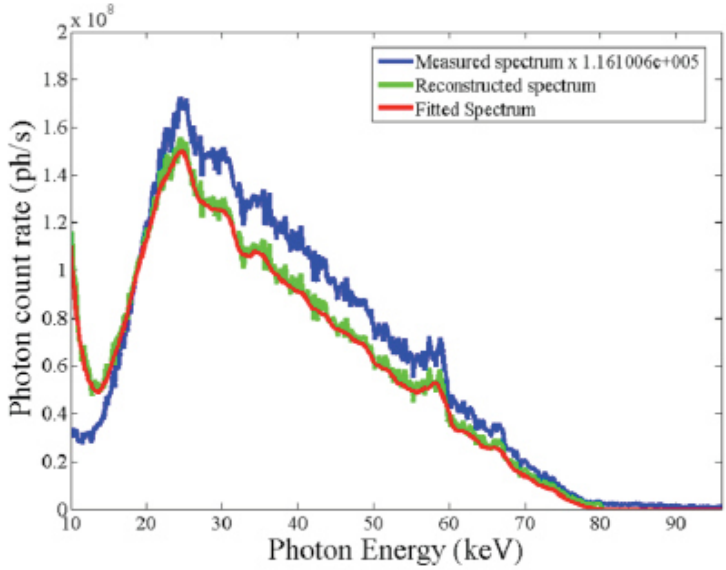

Figure 2: Spectrum of Micro focus X-ray source with voltage set at 80 kV and current at 50 µA. The colors have the same meaning than in the previous figure, with the difference that the spectrum is measured at 2500 mm and no cutoff occurs.

For a self consistent calibration, one needs calibrated sources as well as absolutely calibrated detectors. The detectors used for our calibration of IPs at the ENEA X-ray laboratory were two, one for soft X-rays and one for hard X-rays. SDD spectrometer (Silicon Drift Detector) for the soft X-rays (fig. 3) has active area of 25 mm^2, silicon thickness of 500 μm and energy resolution of 125eV FWHM at 5.89 keV. The SDD is composed by the main detection unit, made by the SDD module, preamplifier and mechanical cooling housing (XGL-SPCM-4110), and by a second unit made by Power Supply, MCA and shaper unit (XGL-MCSHPW-3110). The detector for the hard X-rays (fig. 4) was the CdTe (model AMPETEK\ X-123CdTe), having an active area of 9 mm^2, a 1000 μm semiconductor thickness and a 100 μm Be window. The detector is mounted on a thermoelectric cooler for reducing the electronic noise. It combines, in a single package, the CdTe drift X-ray detector and preamplifier, the digital pulse processor (AMPTEK DP5) and MCA, and the Power Supply (AMPTEK PC5). It works in an energy range of 5÷150 keV with energy resolution less than 1.2 keV FWHM at 122 keV and a count rate less than 2×10^5. They are very useful in order to deduce the real number of photons of a certain energy that have invested their sensitive areas. This is the whole instrumentation used in our absolute calibration experiments of the imaging plates, where every useful and necessary detail has been shown. The experiment consisted of two parts: in the first the IP were exposed to the Moxtex source, i.e. the large-band radiation, in order to measure the minimum and maximum threshold of response to a photon flux averaged on that energy range. In the second part the spectral response is obtained by exposing the IPs to the fluorescence lines of several materials.

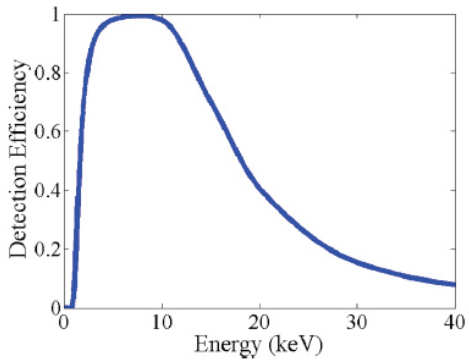

Figure 3: Efficiency curve of the SDD detector versus energy.

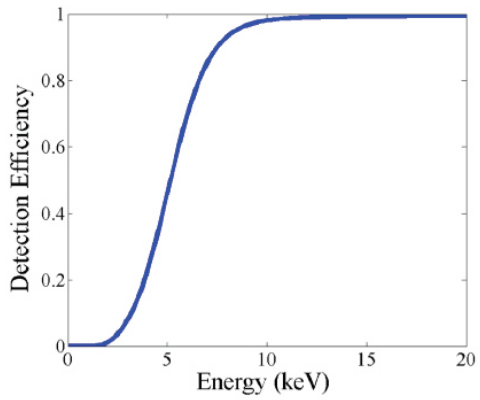

Figure 4: Efficiency curve of the CdTe detector versus energy.

3.2 Spectral calibration of IP through stimulated X-ray fluorescence

The x-ray fluorescence XRF of specimens can be directly excited by *primary photons* from an external source, such as an X-ray tube like those described in subsection 3.1. The XRF stimulated by photons is based on excitation through absorption of radiation and relaxation of a specimen atoms. Photo-absorption is characterized by a complete energy transfer of the photon's energy to the atom, whereby the photon is annihilated. The excited (ionic) atomic state relaxes by refilling the vacancy from an outer shell. This is often associated with the emission of a characteristic photon and the creation of a new vacancy, which is in turn filled from a further outer shell under emission of another photon. This cascade continues until all allowed transitions are exhausted. Finally, a free electron fills the remaining vacancy in an outer shell[14]. With the help of the sources described in the previous section, it's been possible to stimulate fluorescence lines in such a way to measure the spectral response of the IP. In order to stimulate the fluorescence from a core level, radiation at the wavelength corresponding to the ionization of that shell or smaller is needed. That's why we have used the Moxtex source for the stimulation of fluorescence energies up to 40 keV, and the Micro focus for higher energies. The experimental setting in figures 5 and 6 has been set up, with an angle of 90° between the source and the IP, in order to minimize the possibly source signal reaching the imaging plates, which could affect very seriously the measures, being the fluorescence signal low by itself due to the low conversion efficiency from initial radiation into the desired X-ray lines.

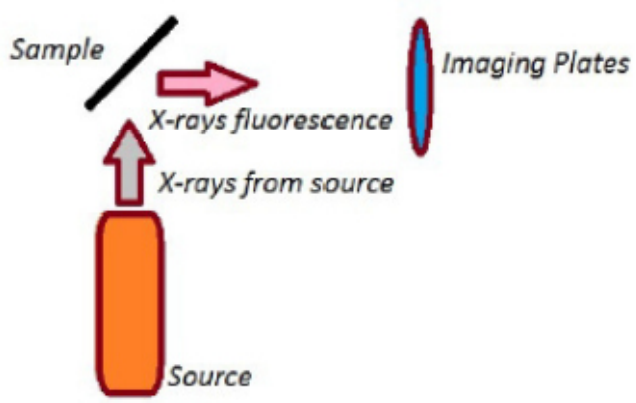

Figure 5: Experimental scheme used for spectral calibration through the stimulation of X-rays fluorescence from various samples.

We have used a set of selected specimens, i.e. their corresponding fluorescence lines (fig. 7) in X-rays range, coming from the transition of the outer electrons into the so called Kα-shells, namely the most inner atomic orbitals, where, according to the spectroscopic notation, K stands for the common 1s level and α_1 and α_2 indicate the level $2p_{3/2}$ and $2p_{1/2}$ respectively, from which electric dipole transitions to the ground are allowed. A particular digression must be done for the BaCs source of X-rays, which, from the table 4, one can see as it emits at 80 keV. This radioactive source emits a narrow line at energy of our interest by means of secondary processes, in fact it is characterized by β-decays: electrons ejected from the nucleus of Cs-137 scatter with the atomic electrons generating the characteristic line at 80 keV.

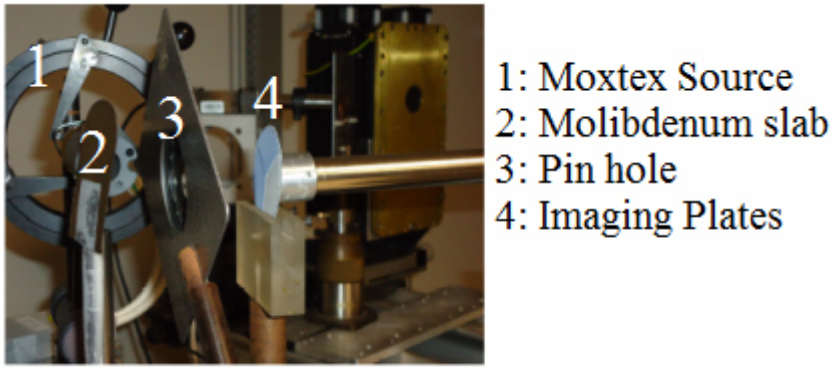

Figure 6: Example (Mo) of X-ray fluorescence experimental setting. The Moxtex source is visible together with the sample and the IP mosaic with the SDD detector behind.

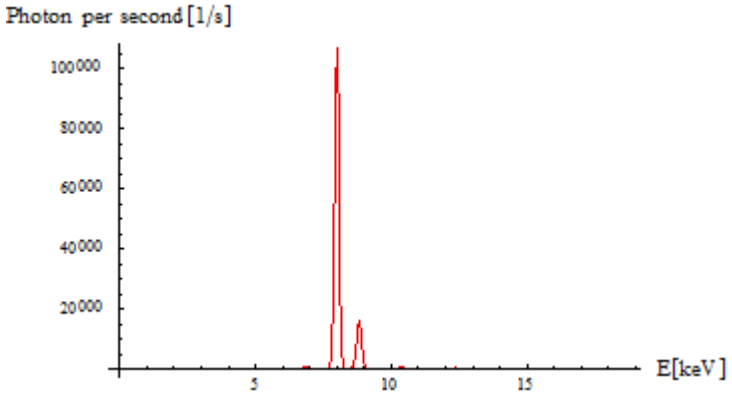

Figure 7: Example (Cu) of measured X-ray fluorescence in photons per second with the SDD detector. Kα and Kβ lines are clearly visible.

Table 4: Fluorescence lines of the selected materials.

Sample	Fluorescence line
Ca	3.6 keV
Cu	8 keV
Mo	17.4 keV
I	28.6 keV
Ta	57 keV
BaCs	80 keV

Before exposing the IP to the X-fluorescence, we have put in their own position (without them) the SDD detector or the CdTe according to the case in which the Moxtex source has been used or the Micro focus, in order to measure the net fluence of photons, namely the number of photons per unit time per unit surface (taking into account the efficiency at a certain photon energy of both semiconductor detectors), in such a way to know the real number of photons impinging on the imaging plates in a given time and to control the quality of fluorescence spectra in that point. A home-made mosaic (fig. 8) of imaging plates of each type (MS, SR, TR)

has been used for our tests, so that a simultaneous analysis with the same experimental setting has been possible for the three types of detectors.

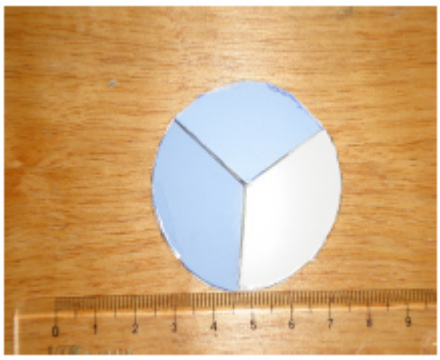

Figure 8: Home-made disk mosaic of imaging plates. The SR type is the top one, the TR on the left and the MS on the right. The dimension scale is reported by the rule on the bottom.

Then we have irradiated our IPs with the different X-ray fluorescence lines, reading the latent images with the appropriate DURR NDT CR35 Bio scanner (fig. 9).

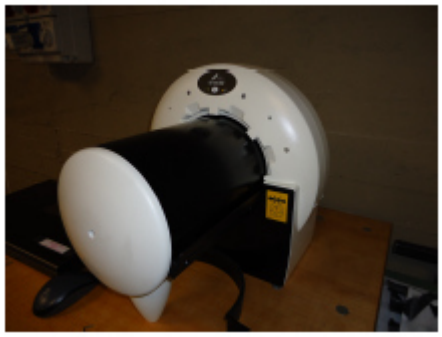

Figure 9: DURR NDT CR35 Bio scanner, used for the reading operation of latent images impressed on the imaging plates.

The amount of luminescence radiation in form of a blue line near 3.2 eV from each pixel is digitized finally forming a gray-level image. The measurements of the Gray Levels (fig. 10) have been done with the freeware software ImageJ; the GL (gray levels) values have been normalized to the number of photons impinged on the detectors in order to make the results comparable among the different type of IP. Thanks to the conversion formula from GL to PSL for this scanner[15] we could express the obtained calibration results directly in terms of PSL values. The errors on the measurements have been estimated with the per cent dispersion of the gray levels in the spots of the IP, due to possible non-uniformity of the fluorescence beam and to lightly non perfect alignments of the imaging plates in the view line of the samples through the diaphragm. In the case of the radioactive BaCs source, which emits another line at 30 keV in addition to that at 80 keV, a 1 mm thin slab of Cu has been positioned between the source and the IP in order to filter out the low energy line. In figure 11,12,13 and 14 we report the experimental results for the spectral calibration of the three different IP types.

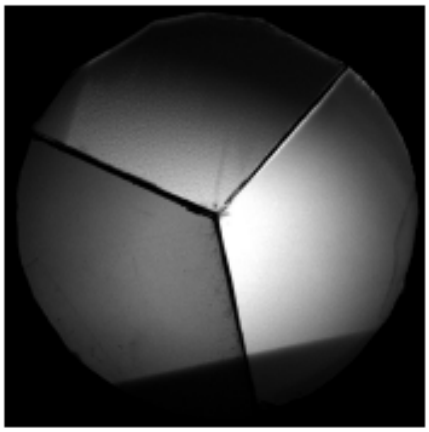

Figure 10: Example (Cu) of digitized gray level image, for exposing 2 minutes.

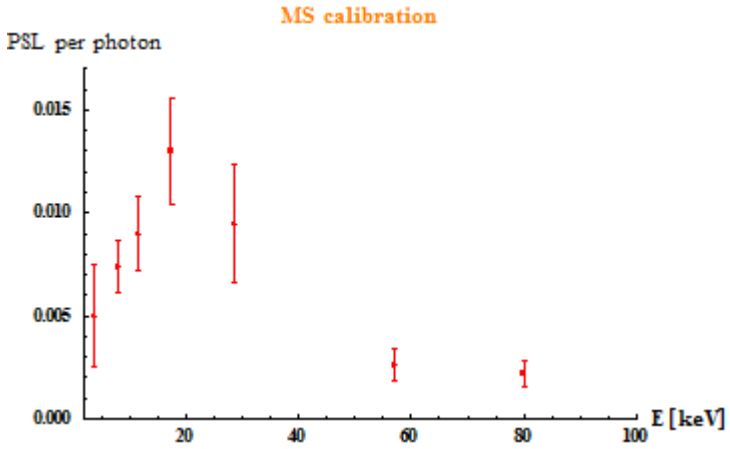

Figure 11: Spectral calibration of the Imaging Plates MS in terms of PSL per photon.

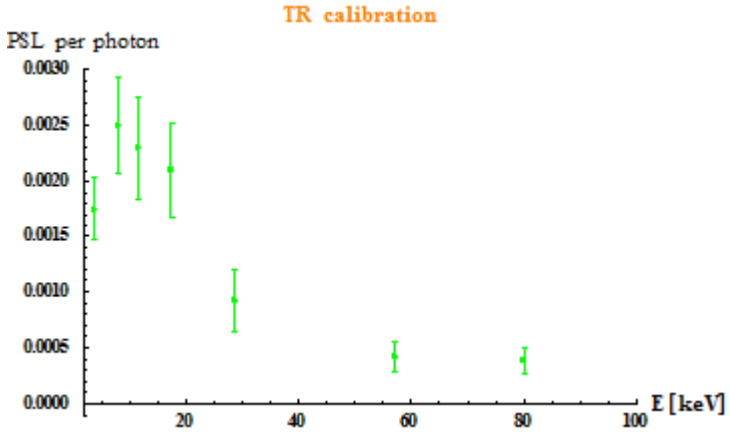

Figure 12: Spectral calibration of the Imaging Plates TR in terms of PSL per photon.

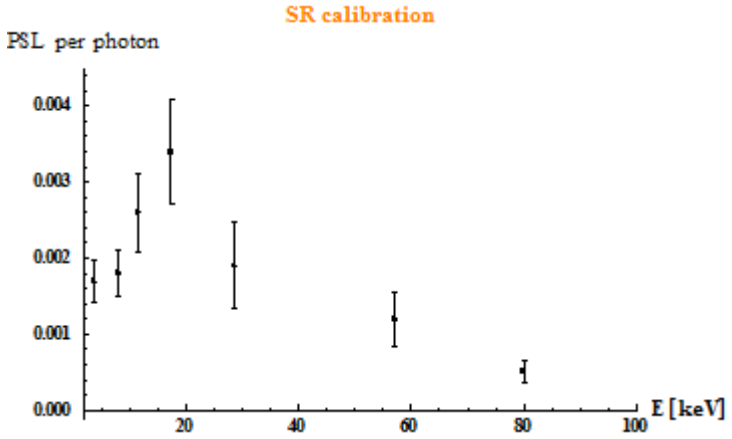

Figure 13: Spectral calibration of the Imaging Plates SR in terms of PSL per photon.

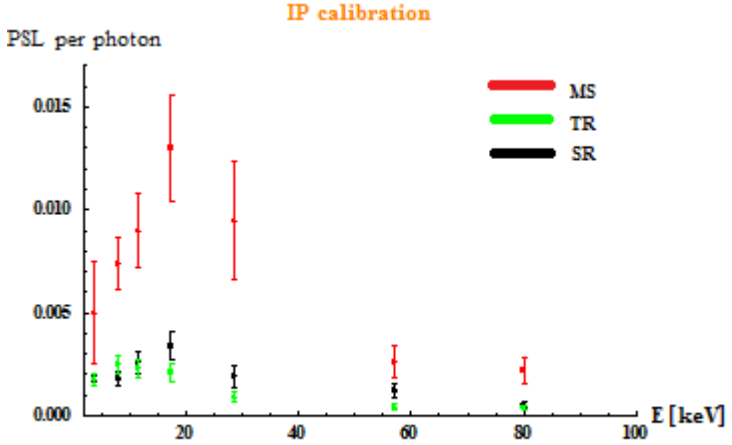

Figure 14: Spectral calibration of the Imaging Plates MS, TR, SR in terms of PSL per photon.

It's worth to analyze the present work with respect to other important works already present in literature [9,10,16]. The interest for imaging plates brought many people for different laboratories to make a calibration of these devices. The response values in fig. 15 are compared with the measurements of Meadowcroft et al. [9] and Maddox et al. [10]. It could be said that there is a very good agreement of measurements of the IP response (PSL/photons) with previous work in the range from 8 keV to 30 keV. There is quite good agreement at low energies (few keV) but the values at higher energies in the present work are lower, showing a significant discrepancy, probably due to the different methodology of calibration with respect to the other works.. The low energy range around 1 keV or below is at the same time very critical and very appealing to study and analyze better with further future calibration works. This range in fact to our knowledge is has been not yet studied, mostly for the reason that it's not easy to find available X-ray sources working within this spectral window.

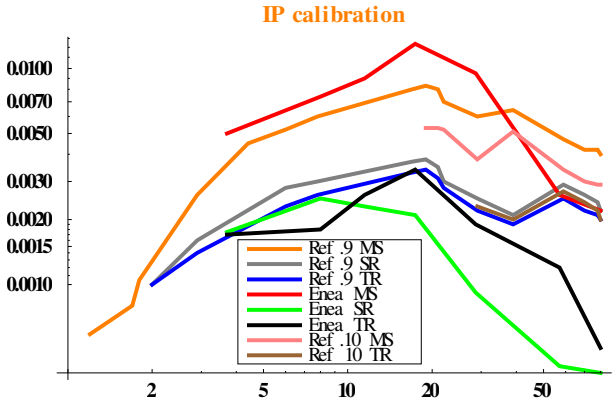

Figure 15: Comparison with ref. [9,10] about IP calibration to X-rays.

3.3 Absolute calibration of IP to X-ray fluence

The response of the imaging plates to the incoming flux of radiation is known from literature [2] to be linear in the number of photons impinging on the plates. We have verified this feature with the help of the Moxtex X-ray source: by varying the supply current one can accelerate more electrons toward the anode, obtaining a greater number of photons as output. We have set the voltage up to 15 kV, in such a way to obtain an X-ray spectrum similar to that represented by the red curve in figure 3, at the exit of the source. A diaphragm (15 mm diameter) is interposed between the source and the IP disk, at a distance of 10 cm from the source and of 6.5 cm from the imaging plates, as in figure 16.

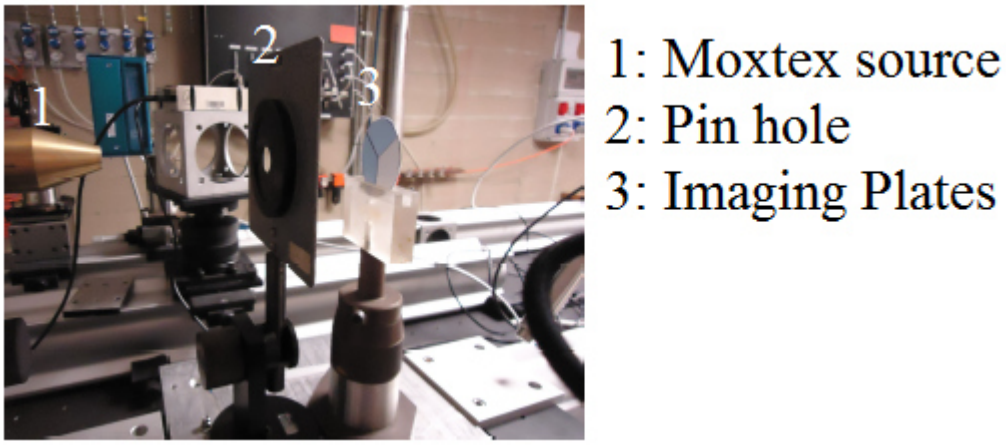

.

Figure 16: Fluence calibration of the imaging plates: experimental setting.

The errors have been evaluated by the fluctuations on the gray levels on the image read with ImageJ. The maximum gray level was 65535, the minimum 0, which indicate the levels of saturation. The flux has been estimated by the remote software of the Moxtex source,

considering the presence of the diaphragm and its dimension, then have been measured for a further confirmation with the help of the SDD detector. Results are showed in figures 17, 18 and 19.

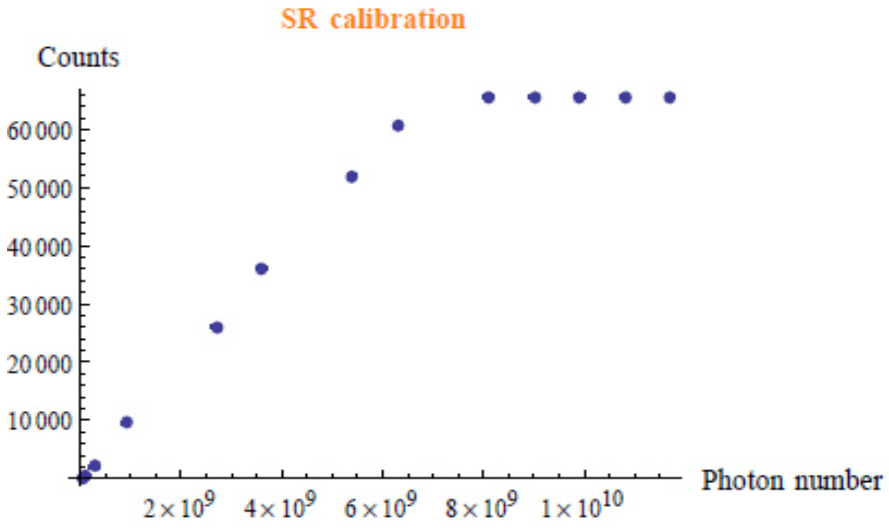

Figure 17: Fluence calibration of the imaging plates: SR type.

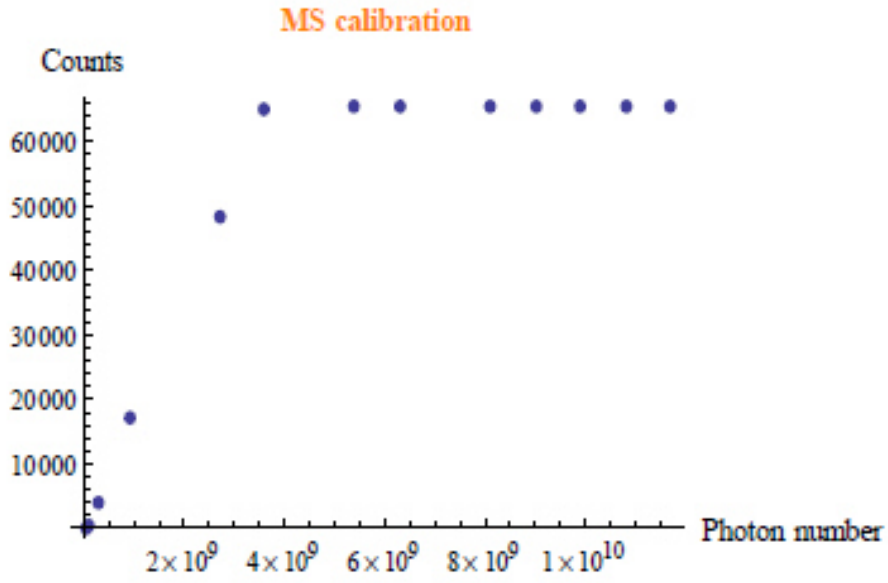

Figure 18: Fluence calibration of the imaging plates: MS type.

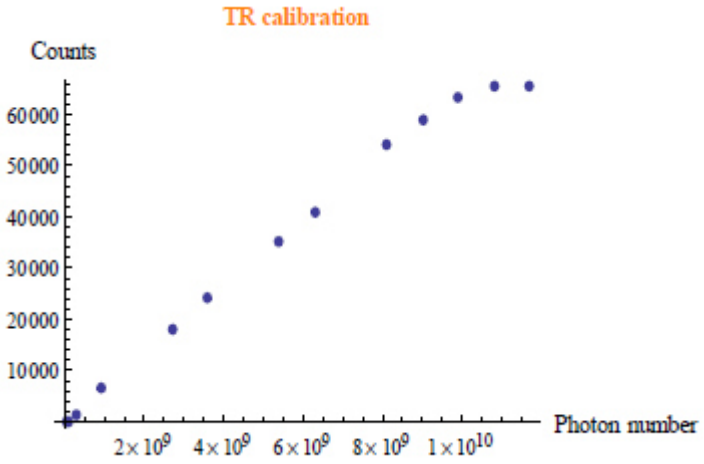

Figure 19: Fluence calibration of the imaging plates: TR type.

The MS type is the most sensitive to radiation, then the SR and finally the TR come. Basically this is due to the different mylar (absent in TR type) and phosphor layer thicknesses among the different IP. The mylar layer acts like a good X-ray absorber, nevertheless even without mylar layer, the TR type doesn't have the best sensitivity because of the reduced phosphor layer. Furthermore it must be considered that the phosphor composition is different in the SR type with respect to the others. There is not so many work done for imaging plates to our knowledge about the response to photon or particle fluxes in order to quantitatively understand the dynamical range of these detectors. The present measurements here were taken sending a photon spectrum centered at 8 keV, but the linear response in different spectral ranges is expected different. Could be good to know the linear response for higher and lower photon energies, therefore this could be the aim for future calibration campaigns.

Conclusions

An absolute calibration to X-rays of the Imaging Plates detectors has been performed and the results have been showed. The spectral response of the IP in the X-ray range 1÷100 keV and the IP optical density in the X-ray range 1÷15 keV have been investigated.

References

[1] Thoms, M., von Seggern, H., Winnacker, A., *Spatial correlation and photostimulability of defect centers in the x-ray storage phosphor BaFBr:Eu*$^{2+}$. Phys. Rev. B 44, 17 (1991).

[2] von Seggern, H. *X-ray imaging with photostimulable phosphors*. Nuclear Instruments and Methods in Physics Research A322 467-471 (1992).

[3] K. A. Tanaka, T. Yabuuchi, T. Sato, R. Kodama, Y. Kitagawa T. Takahashi,T. Ikeda, Y. Honda, and S. Okuda, Rev. Sci. Instrum. **76**, 013507 (2005).

[4] A. Mancic, J. Fuchs, P. Antici, S. A. Gaillard, and P. Audebert, Rev. Sci.Instrum. **79**, 073301 (2008).

[5] C. G. Freeman, G. Fiksel, C. Stoeckl, N. Sinenian, M. J. Canfield, G. B.Graeper, A. T. Lombardo, C. R. Stillman, S. J. Padalino, C. Mileham, T. C. Sangster, and J. A. Frenje, Rev. Sci. Instrum. **82**, 073301 (2011).

[6] I. W. Choi, C. M. Kim, J. H. Sung, I. J. Kim, T. J. Yu, S. K. Lee, Y.-Y. Jin,K. H. Pae, N. Hafz, and J. Lee, Meas. Sci. Technol. **20**, 115112 (2009).

[7] H.Chen , N. L. Back, T. Bartal, F. N. Beg, D. C. Eder, A. J. link, A. G. MacPhee, Y. Ping, P. M. Song, A. Throop, and L. Van Woerkom, and L. Van Woerkom, Rev. Sci.Instrum. **79**, 033301 (2008).

[8] Bonnet, T., Comet, M., Denis-Petit, D., Gobet, F.,Hannachi, F. et al. *Response function of Fuji imaging plates to monoenergetic protons in the energy range 0.6-3.2 MeV*. Rev. Sci. Instrum. **84**, 013508 (2013).

[9] A. L. Meadowcroft, C. D. Bentley, and E. N. Stott, Rev. Sci. Instrum. **79**, 113102 (2008).

[10] B. R. Maddox, H. S. Park, B. A. Remington, N. Izumi, S. Chen, C. Chen, G. Kimminau, Z. Ali, M. J. Haugh, and Q. Ma, Rev. Sci. Instrum. **82**, 023111 (2011).

[11] Bonnet, T., Comet, M., Denis-Petit, D., Gobet, F.,Hannachi, F. et al. *Response functions of imaging plates to photons, electrons and 4he particles.* Rev. Sci. Instrum. **84**, 103510 (2013).

[12] Sidky, E. Y. et al., *A robust method of X-ray source spectrum estimation from transmission measurements: Demonstrated on computer simulated, scatter-free transmission data*. Journal of Applied Physics, **97**, 124701 (2005)

[13] Pacella, D., Romano, A., Lee, S., Causa, F., Gabellieri, L., Choe, W., *Self consistent calibration of detectors and sources for Hard and Soft X-ray diagnostics.* Modern Instrumentation, (2014).

[14] B. Beckhoff et al., *Handbook of Practical X-Ray Fluorescence Analysis*, Springer-Verlag Berlin Heidelberg (2006)

[15] Ingenito et al, *Comparative calibration of IP scanning equipment,* submitted to JINST PPLA 2015 Conference Proceedings

[16] G. Boutoux et al., submitted to Rev. Sci. Instrum. (2015)